Spring 2024

A free-boundary successive over-relaxation Grad-Shafranov Equation Solver

Alec J. Damsell
University of New Hampshire

A FREE-BOUNDARY SUCCESSIVE OVER-RELAXATION GRAD-SHAFRANOV EQUATION SOLVER

BY

Alec J. Damsell

THESIS

Submitted to the University of New Hampshire

in Partial Fulfillment of

the Requirements for the Degree of

Bachelor's of Science

in

Physics

May 15, 2024

TABLE OF CONTENTS

ABSTRACT

A FREE-BOUNDARY SUCCESSIVE OVER-RELAXATION GRAD-SHAFRANOV EQUATION SOLVER

by

Alec J. Damsell

University of New Hampshire, May, 2024

Fusion has long been considered the "Holy Grail" of renewable energy, but has not yet seen viability as a commercial power source. With tokamaks like SPARC, NSTX-U, and ITER coming online over the next ten years, there is growing investment in fusion technology by both the public and private sector. If these tokamaks reach or exceed their scientific aims, further investment in fusion and new tokamak designs are expected. The first step in designing a tokamak is choosing a good plasma equilibrium, which is described by the Grad-Shafranov equation. This work presents a successive over-relaxation routine to solve the Grad-Shafranov equation. This work also presents the implementation of additional routines to modify the successive over-relaxation code into a free-boundary Grad-Shafranov equation solver. The successive over-relaxation routine showed good agreement with analytical solutions. Ultimately, this tool serves as a good starting point for testing plasma equilibria for a given coil and solenoid configuration in the early design phase of tokamaks.

CHAPTER 1

Introductory Plasma Physics

Plasma is the so-called fourth state of matter. We are all familiar with solids, liquids, and gases, as they are present in our daily lives. Plasmas, however, are not so familiar. In essence, a plasma is a gas that has been energized such that electrons decouple from their atomic nuclei, forming two charged-particle populations. A condition that is common in plasma environments is quasi-neutrality, which states that the sum of all positive and negative charges is equal to zero. This chapter will cover some of the basic equations that govern plasma physics, as well as drifts, adiabatic invariants, and characteristic time scales.

1.1 Single Particle Motion

All plasmas consist of particles that have electric charge. As such, each particle is coupled with its neighbors via the Coulomb force

$$\vec{F}_c = q\vec{E}, \tag{1.1}$$

where q is the charge of the particle being acted upon by the Coulomb force and $\vec{E}$ is the electric field vector [1]. The electric field from a single point charge is

$$\vec{E} = \frac{1}{4\pi\epsilon_0}\frac{q'}{r^2}\hat{r}, \tag{1.2}$$

where q' is the charge of the particle emitting the field, r is the distance from the charge, and $\hat{r}$ is the radial unit vector in spherical coordinates [2]. Given that particles can vary wildly

in position, trying to calculate the net electric field on a single particle from the remaining population is computationally costly and overly complicated. If these charges are moving, there are also changing magnetic fields that will also impart forces [2]. There are frameworks through which large plasma environments can be modeled with comparative ease, but for now, it is best to focus on the single-particle case.

The Lorentz force, which is the force on a single charged particle from external electromagnetic fields, is

$$\vec{F} = q(\vec{E} + \vec{v} \times \vec{B}), \tag{1.3}$$

where $\vec{v}$ is the velocity of the particle and $\vec{B}$ is the magnetic-field vector[1]. Assuming for now that $|\vec{E}| = 0$, the Lorentz force equation becomes

$$\vec{F} = q\vec{v} \times \vec{B}. \tag{1.4}$$

By the definition of the cross product, $\vec{F}$ acts perpendicularly to both $\vec{v}$ and $\vec{B}$, and gives rise to circular motion in the plane perpendicular to $\vec{B}$ [1]. This circular motion is called gyromotion. By using the equations of uniform circular motion along with Eq. 1.4, two important quantities, the gyrofrequency and the gyroradius, can be derived [1–3]. The gyrofrequency, ω_g, is

$$\omega_g = \frac{|q|B_0}{m}, \tag{1.5}$$

where m is the particle's mass. The gyroradius (also called the Larmor radius) is

$$r_g = \frac{mv_\perp}{|q|B_0}. \tag{1.6}$$

Given these quantities, an equation for the particle's position can be found. For a particle of charge, q, mass, m, with initial velocity, $v_0\hat{y}$, in a uniform magnetic field, $-B_0\hat{z}$, located

[1] If $|\vec{B}| = 0$, Eq. 1.3 becomes Eq. 1.1.

at the origin, its position can be described by

$$\vec{r}(t) = r_g[\mp 1 \pm \cos(\omega_g t)]\,\hat{x} + r_g \sin(\omega_g t)\,\hat{y}, \tag{1.7}$$

where the signs of the x-component depend on whether the charge, q, is positive or negative [3].

1.2 Drifts

The motion of charged particles in uniform magnetic fields is relatively simple, but things get a bit trickier with the reintroduction of the electric field. Assuming that the fields are perpendicular to each other (e.g. $\vec{E} = E_0\hat{z},\ \vec{B} = B_0\hat{x}$), and the particle resides in the yz-plane with a velocity vector of $(0, \dot{y}, \dot{z})$, where the dots denote a time derivative of position, finding the equations of motion requires evaluating the cross product of $\vec{v}$ and $\vec{B}$

$$\begin{vmatrix} \hat{x} & \hat{y} & \hat{z} \\ 0 & \dot{y} & \dot{z} \\ B_0 & 0 & 0 \end{vmatrix} = \dot{z}B_0\hat{y} - \dot{y}B_0\hat{z}. \tag{1.8}$$

Taking the right hand side and adding the Coulomb force yields

$$\vec{F} = m\vec{a} = q[\dot{z}B_0\hat{y} + (E_0 - \dot{y}B_0)\hat{z}]. \tag{1.9}$$

Separating it by component, the equations of motion become

$$m\ddot{y} = qB_0\dot{z}, \quad m\ddot{z} = qE_0 - qB_0\dot{y}, \tag{1.10}$$

which gives rise to a general solution of the form

$$y(t) = C_1 \cos \omega_g t + C_2 \sin \omega_g t + (E_0/B_0)t + C_3 \tag{1.11}$$

$$z(t) = C_2 \cos \omega_g t - C_1 \sin \omega_g t + C_4, \tag{1.12}$$

which is harder to work with than the result in Eq. 1.7 [2]. By deciding that the particle starts at rest at the origin and making some substitutions, Eqs. 1.11 and 1.12 can be written as an equation of a circle

$$\left(y - \frac{E_0}{B_0}t\right)^2 + \left(z - \frac{E_0}{\omega_g B_0}\right)^2 = \frac{E_0^2}{\omega_g^2 B_0^2}, \tag{1.13}$$

where the center of the circle drifts at a constant rate in the y-direction [2]. This constant drift velocity is why it is useful to think of drifts as affecting the point in the center of a particle's gyromotion. Instead of mapping out a particle's trajectory using Eqs. 1.11 and 1.12, the $\vec{E} \times \vec{B}$ drift affecting the guiding center of a particle can be written as

$$\vec{v}_{E\times B} = \frac{\vec{E} \times \vec{B}}{B^2}. \tag{1.14}$$

Something that seems peculiar at first glance is that ions and electrons will drift in the same direction and at the same speed, independent of charge or mass. This is a property exclusive to the $\vec{E} \times \vec{B}$ drift. Much of this chapter has relied upon examples with specific orientations of the electric and magnetic fields, as well as the velocity of a single charged particle. Before covering other drifts, let's generalize the velocity of a single particle a bit more.

In Cartesian coordinates, a single particle can have an arbitrary velocity vector

$$\vec{v} = v_x \hat{x} + v_y \hat{y} + v_z \hat{z}. \tag{1.15}$$

If the magnetic field is in the $\hat{z}$ direction, the z-component of the particle's velocity is parallel to the magnetic field. Updating the notation for Eq. 1.15 yields

$$\vec{v} = v_x\hat{x} + v_y\hat{y} + \vec{v}_{\parallel}. \tag{1.16}$$

Since a magnetic field does no work (the magnetic force is always perpendicular to the path traveled) it is convenient to group the x and y components of the velocity together into one term, $\vec{v}_{\perp}$, thus

$$\vec{v} = \vec{v}_{\perp} + \vec{v}_{\parallel}, \tag{1.17}$$

where $|\vec{v}_{\perp}| = \sqrt{v_x^2 + v_y^2}$. This more general form of relating the velocity of a particle to the external magnetic field makes the following drift equations more applicable to a variety of field and particle configurations. Below are some other drifts with a sentence or two explaining how they arise. For a more thorough derivation, see chapter 2 of Kallenrode's *Space Physics*.

The $\vec{F} \times \vec{B}$ drift is caused by a general force, $\vec{F}$ acting perpendicular to $\vec{B}$ [3]. A heuristic derivation of this equation is done by substituting $\vec{F} = \vec{E}q$ into Eq. 1.14, yielding

$$\vec{v}_F = \frac{1}{q}\frac{\vec{F} \times \vec{B}}{B^2}. \tag{1.18}$$

In an inhomogeneous magnetic field, the gradient of the magnetic field causes a drift called the grad-B drift given by

$$\vec{v}_{\nabla B} = \frac{mv_{\perp}^2}{2qB}\frac{\vec{B} \times \nabla B}{B^2} = \pm\frac{v_{\perp} r_L}{2B^2}\vec{B} \times \nabla B. \tag{1.19}$$

The curvature drift is caused by the fictitious centrifugal force that a particle feels in a curved magnetic field [3]. The velocity from the curvature drift is

$$\vec{v}_R = \frac{mv_{\parallel}^2}{qB^2}\frac{\vec{R}_{\mathrm{c}} \times \vec{B}}{R_{\mathrm{c}}^2}, \tag{1.20}$$

where $\vec{R}_{\rm c}$ is the radius of curvature of the magnetic-field line [3]. In vacuum, Eqs. 1.19 and 1.20 can be combined into

$$\vec{v}_{\nabla B} + \vec{v}_R = \frac{m}{q}\frac{\vec{R}_{\rm c} \times \vec{B}}{R_{\rm c}^2 B^2}\left(v_\perp^2 + \frac{1}{2}v_\parallel^2\right). \tag{1.21}$$

1.3 Adiabatic Invariants

Adiabatic invariants are quantities that are nearly exactly conserved by oscillating particles in slowly varying systems. In particular, adiabatic invariants are nearly exactly conserved when the period of oscillation is much smaller than the time scale on which the system varies. For charged particles gyrating in a magnetic field, the first adiabatic invariant is the magnetic moment, μ, defined as

$$\mu = \frac{mv_\perp^2}{2B} = \frac{K_\perp}{B} \tag{1.22}$$

where $K_\perp$ is the particle's kinetic energy from gyromotion. As B changes, $K_\perp$ changes proportionally to keep μ constant [3, 4].

The second adiabatic invariant is the longitudinal invariant, which states that

$$J = \oint mv_\parallel \, {\rm d}s. \tag{1.23}$$

For J to remain constant, the time scale of fluctuations in the magnetic field must be much longer than the period of the particle's bounce motion [5].

The third adiabatic invariant is the flux invariant. The magnetic flux, Φ, through a particle's drift orbit is

$$\Phi = \oint mv_{\rm d} r \, {\rm d}\psi, \tag{1.24}$$

where v_d is the drift velocity, r is the radius of the drift orbit, and ψ is the azimuthal angle [3]. For Φ to remain invariant, fluctuations in the magnetic field must have a much longer time scale than the drift orbit period [5].

1.4 Characteristic Scales

An important length scale to plasma environments is the Debye length. The Debye length is the distance at which a single charge's electric field is completely shielded by particles of opposite charge in a process called Debye shielding. The Debye length for a given plasma is

$$\lambda_{\mathrm{D}} = \sqrt{\frac{3\epsilon_0 k_{\mathrm{b}} T}{e^2 n_{\mathrm{e}}}}, \tag{1.25}$$

where e is the elementary charge and n_{e} is the electron number density [3].

Plasmas also oscillate. If the net charge of a large quasineutral plasma population experiences a perturbation, the neighboring particles will try to push or pull (depending on charge) back towards equilibrium. Often, these perturbations ripple throughout the entire collection of charged particles, causing a larger oscillation. The plasma frequency, ω_{pe} of a given plasma is

$$\omega_{\mathrm{pe}} = \sqrt{\frac{n_{\mathrm{e}} e^2}{\epsilon_0 m_{\mathrm{e}}}}, \tag{1.26}$$

where m_{e} is the mass of an electron [3]. These characteristic length and time scales can help determine which numerical methods and mathematical frameworks one should use to study a given plasma environment. For the case of magnetic confinement fusion and this document, magnetohydrodynamics is the primary focus.

CHAPTER 2

Magnetohydrodynamics

Magnetohydrodynamics (MHD) is a set of closed equations for describing plasma systems where the time and length scales of interest are much larger than the Debye length, gyroradius, mean-free-path, gyroperiod, collision time, and plasma oscillation period. The focus of this chapter is to discuss and derive the equations of ideal MHD, derive the Grad-Shafranov equation, as well as derive an equation for the Shafranov shift in the limit of large aspect ratio.

2.1 Deriving Ideal MHD

2.1.1 The Fluid Equations

The *hydrodynamics* aspect of magnetohydrodynamics refers to a fluid. As such, the equations that govern how the plasma moves come from conservation of mass, momentum, and energy from fluid mechanics. First, I will derive the mass-conservation equation in a similar manner to Euler [6], then using a more rigorous approach as shown in Landau and Lifshitz [7], which is used for momentum and energy conservation.

First, let the fluid be of arbitrary density and velocity at all points in space and time, $\rho(t,x,y,z)$, $\vec{u}(t,x,y,z)$[1]. Next, assume that there is an infinitesimal volume, with dimensions $\mathrm{d}x \times \mathrm{d}y \times \mathrm{d}z$. The amount of fluid flowing into the box can be written as

$$\text{fluid in} = \rho u_x \mathrm{d}y\mathrm{d}z + \rho u_y \mathrm{d}x\mathrm{d}z + \rho u_z \mathrm{d}x\mathrm{d}y \tag{2.1}$$

[1]It is convention to use u to describe the velocity of fluids.

where $v_x,\ v_y\ v_z$ are the components of velocity perpendicular to the left, front, and bottom sides of the box, respectively. The fluid flowing out of the box can be written similarly with a Taylor expansion, giving rise to

$$\text{fluid out} = (\rho u_x + \frac{\partial}{\partial x}\rho u_x \mathrm{d}x)\mathrm{d}y\mathrm{d}z + (\rho u_y + \frac{\partial}{\partial y}\rho u_y \mathrm{d}y)\mathrm{d}x\mathrm{d}z + (\rho u_z + \frac{\partial}{\partial z}\rho u_z \mathrm{d}z)\mathrm{d}x\mathrm{d}y. \quad (2.2)$$

The accumulation of fluid in the volume can be written as

$$\frac{\partial \rho}{\partial t}\mathrm{d}x\mathrm{d}y\mathrm{d}z = \text{fluid in} - \text{fluid out}. \quad (2.3)$$

Finally, plugging Eqs. 2.1 and 2.2 into Eq. 2.3 yields

$$\frac{\partial \rho}{\partial t}\mathrm{d}x\mathrm{d}y\mathrm{d}z = -\frac{\partial}{\partial x}\rho u_x \mathrm{d}x\mathrm{d}y\mathrm{d}z - \frac{\partial}{\partial y}\rho u_y \mathrm{d}x\mathrm{d}y\mathrm{d}z - \frac{\partial}{\partial z}\rho u_z \mathrm{d}x\mathrm{d}y\mathrm{d}z, \quad (2.4)$$

which can be rewritten into the continuity equation,

$$\frac{\partial \rho}{\partial t} + \nabla \cdot (\rho \vec{u}) = 0. \quad (2.5)$$

While Euler's approach makes for a good heuristic method, it relies on a less-than-arbitrary choice of volume. An approach using Gauss' theorem is more robust and has the added benefit of being the same mathematical tool needed to derive the momentum equation and the energy equation. First, let's say that the mass inside of an arbitrary volume is given by

$$M = \int_V \rho \ \mathrm{d}V. \quad (2.6)$$

Assuming that the volume stays fixed, the change in mass over time can be described by the amount of fluid passing through the surface, S, that bounds the volume. This results in

$$\frac{\mathrm{d}M}{\mathrm{d}t} = \int_V \frac{\partial \rho}{\partial t}\ \mathrm{d}V = -\int_S \rho \vec{u} \cdot \mathrm{d}\vec{S} + f, \quad (2.7)$$

where f acts as a source or sink term. Neglecting f for now and using Gauss' theorem on the rightmost side of Eq, 2.7 yields

$$\int_S \rho\vec{u} \cdot \mathrm{d}\vec{S} = \int_V \nabla \cdot (\rho\vec{u})\, \mathrm{d}V, \tag{2.8}$$

thus,

$$\frac{\partial \rho}{\partial t} + \nabla \cdot (\rho\vec{u}) = 0. \tag{2.9}$$

So long as any quantity is conserved in an arbitrary fluid volume, it will be conserved in the entire fluid. Using Eqs. 2.7 and 2.8 and generalizing for an arbitrary conserved density (mass, momentum, energy, etc.), α, is

$$\int_V \frac{\partial \alpha}{\partial t}\, \mathrm{d}V = -\int_V \nabla \cdot (\alpha\vec{u})\, \mathrm{d}V + f. \tag{2.10}$$

To find the equivalent of Newton's second law for a fluid, $\alpha = \rho\vec{u}$. Following a similar procedure for mass conservation the resulting equation for momentum conservation is

$$\rho\left(\frac{\partial \vec{u}}{\partial t} + \vec{u} \cdot \nabla\vec{u}\right) = -\nabla p + \nabla\overleftrightarrow{\sigma} + \vec{f}_{\mathrm{ext}}, \tag{2.11}$$

where $\overleftrightarrow{\sigma}$ is the viscous stress tensor, p is a scalar pressure, and $\vec{f}_{ext}$ are any external forces on the fluid [7]. The same can be done for energy, using $\alpha = \frac{1}{2}\rho u^2 + e$, where e is the internal energy and $\frac{1}{2}\rho u^2$ is the kinetic energy. Using the same formalism as before, we can find that the conservation of energy in a fluid is written as

$$\frac{\partial}{\partial t}\left(\frac{1}{2}\rho u^2 + e\right) = -\nabla\left[\vec{u}\left(\frac{1}{2}\rho u^2 + p + e\right)\right] + \nabla \cdot (\overleftrightarrow{\sigma} \cdot \vec{u}) + \vec{f} \cdot \vec{u} - \nabla \cdot \vec{q}, \tag{2.12}$$

where $\vec{q}$ is the heat flux [7]. Eqs. 2.9, 2.11, and 2.12 are the fundamental equations of fluid mechanics.

2.1.2 Maxwell's Equations

Maxwell's equations are a coupled set of partial differential equations that form the foundation for classical electrodynamics. In SI units, the differential form of Maxwell's equations is

$$\begin{aligned} \nabla \cdot \vec{E} &= \frac{\rho}{\varepsilon_0} \\ \nabla \cdot \vec{B} &= 0 \\ \nabla \times \vec{E} &= -\frac{\partial \vec{B}}{\partial t} \\ \nabla \times \vec{B} &= \mu_0 \left(\vec{J} + \varepsilon_0 \frac{\partial \vec{E}}{\partial t} \right), \end{aligned} \tag{2.13}$$

where $\vec{J}$ is the current density, and ε_0 and μ_0 are the vacuum permittivity and vacuum permeability, respectively [2]. The permeability and permittivity of free space are related to the propagation speed of an electromagnetic wave by

$$c^2 = \frac{1}{\varepsilon_0 \mu_0}. \tag{2.14}$$

These equations describe not only how currents and charge densities generate electric and magnetic fields, but also how fluctuations in these fields impact one another.

2.1.3 Ohm's Law

The last piece needed to complete the set of MHD equations is the generalized Ohm's law, given by

$$\vec{E} + \vec{u} \times \vec{B} = \eta \vec{J} \tag{2.15}$$

where η is the resistivity of the plasma [3].

2.1.4 Completing the Set of Ideal MHD Equations

Tying together the various subsections of this chapter, the full set of MHD equations are

$$\frac{\partial \rho}{\partial t} + \nabla \cdot (\rho \vec{u}) = 0$$

$$\rho \left(\frac{\partial \vec{u}}{\partial t} + \vec{u} \cdot \nabla \vec{u} \right) = -\nabla p + \nabla \overleftrightarrow{\sigma} + \vec{J} \times \vec{B} + \vec{f}_{\text{ext}}$$

$$\frac{\partial}{\partial t} \left(\frac{1}{2} \rho u^2 + e \right) = -\nabla \left[\vec{u} \left(\frac{1}{2} \rho u^2 + p + e \right) \right] + \nabla \cdot (\overleftrightarrow{\sigma} \cdot \vec{u}) + \vec{f} \cdot \vec{u} - \nabla \cdot \vec{q}$$

$$\nabla \cdot \vec{E} = \frac{\rho}{\varepsilon_0}$$

$$\nabla \cdot \vec{B} = 0$$

$$\nabla \times \vec{E} = -\frac{\partial \vec{B}}{\partial t}$$

$$\nabla \times \vec{B} = \mu_0 \left(\vec{J} + \varepsilon_0 \frac{\partial \vec{E}}{\partial t} \right)$$

$$\vec{E} + \vec{u} \times \vec{B} = \eta \vec{J}.$$

In the two-fluid model of MHD, the electron and ion populations are governed by their own set of MHD equations [8]. These can be simplified by approximating the plasma as a single charged fluid. As covered in chapter 1, for long length scales, the plasma can be treated as quasi-neutral, meaning that $\nabla \cdot \vec{E} = 0$. Next, the energy equation can be simplified by using the first law of thermodynamics and arguing that energy is conserved except for $p\mathrm{d}V$ work [7]. The final approximations are that the resistivity of the plasma is small and that $\mu_0 \varepsilon_0 (\partial \vec{E}/\partial t)$ is small relative to $\mu_0 \vec{J}$. The final set of ideal MHD equations for a single

fluid is then

$$\begin{aligned}
\frac{\partial \rho}{\partial t} + \nabla \cdot (\rho \vec{u}) &= 0 \\
\rho \left(\frac{\partial \vec{u}}{\partial t} + \vec{u} \cdot \nabla \vec{u} \right) &= -\nabla p + \vec{f}_{\text{ext}} \\
\frac{\partial e}{\partial t} + \nabla \cdot (e \vec{u}) &= -p \nabla \cdot \vec{u} \\
\nabla \cdot \vec{B} &= 0 \\
\nabla \times \vec{E} &= -\frac{\partial \vec{B}}{\partial t} \\
\nabla \times \vec{B} &= \mu_0 \vec{J} \\
\vec{E} + \vec{u} \times \vec{B} &= 0.
\end{aligned} \tag{2.16}$$

2.2 Deriving the Grad-Shafranov Equation

The Grad-Shafranov equation is an axisymmetric equilibrium equation in MHD[2] [9, 10]. The derivation starts with setting the left-hand side of the momentum equation to zero and using the Lorentz force for $\vec{f}_{ext}$ such that

$$0 = -\nabla p + \vec{J} \times \vec{B}. \tag{2.17}$$

Using Ampere's Law to solve for $\vec{J}$, we can rewrite Eq. 2.17 as

$$0 = -\nabla p + \frac{1}{\mu_0} (\nabla \times \vec{B}) \times \vec{B}. \tag{2.18}$$

It is then useful to rewrite $\vec{B}$ in terms of the vector potential, $\vec{A}$ in cylindrical coordinates

$$\nabla \times \vec{B} = \hat{R} \left(\frac{1}{R} \frac{\partial A_Z}{\partial \varphi} - \frac{\partial A_\varphi}{\partial Z} \right) + \hat{\varphi} \left(\frac{\partial A_R}{\partial Z} - \frac{\partial A_Z}{\partial R} \right) + \hat{Z} \left[\frac{1}{R} \frac{\partial}{\partial R} (R A_\varphi) - \frac{1}{R} \frac{\partial A_R}{\partial \varphi} \right]. \tag{2.19}$$

[2]Plasma equilibria in magnetic fields were calculated by Grad and Rubin (1958) and Shafranov (1966). Unfortunately, the name, "Grad-Rubin-Shafranov equation" never caught on. Thus, Rubin's contributions are acknowledged in the footnote of this undergraduate thesis.

By axisymmetry, all partial derivatives with respect to φ are zero. The substitution, $\psi = RA_\varphi$ is made, and the $\hat{\varphi}$ component is set equal to B_{T}. Eq. 2.19 simplifies to

$$\vec{B} = -\frac{\hat{R}}{R}\frac{\partial\psi}{\partial Z} + RB_{\mathrm{T}}\frac{\hat{\varphi}}{R} + \frac{\hat{Z}}{R}\frac{\partial\psi}{\partial R}. \tag{2.20}$$

Next, we replace RB_{T} with a free function, F, leading to

$$\vec{B} = -\frac{\hat{R}}{R}\frac{\partial\psi}{\partial Z} + F\frac{\hat{\varphi}}{R} + \frac{\hat{Z}}{R}\frac{\partial\psi}{\partial R}. \tag{2.21}$$

Using vector identities and the cross product, We can rewrite Eq. 2.21 as

$$\vec{B} = \frac{\partial\psi}{\partial Z}\frac{\hat{Z}\times\hat{\varphi}}{R} + \frac{\partial\psi}{\partial R}\frac{\hat{R}\times\hat{\varphi}}{R} + F\nabla\varphi. \tag{2.22}$$

By grouping like terms, we can simplify Eq. 2.22 to the form

$$\vec{B} = \nabla\psi\times\nabla\varphi + F\nabla\varphi. \tag{2.23}$$

Using Eq 2.23 and various vector calculus identities, $\nabla\times\vec{B}$ can evaluated as

$$\nabla\times\vec{B} = \nabla\psi\cdot\underset{1}{\nabla}(\nabla\varphi) + \nabla\varphi\cdot\underset{2}{\nabla}(\nabla\psi) - \nabla\varphi(\underset{3}{\nabla}\cdot\nabla\psi) + \nabla\psi(\underset{4}{\nabla}\cdot\nabla\varphi) + \frac{\mathrm{d}F}{\mathrm{d}\psi}\underset{5}{\nabla\psi}\times\nabla\varphi. \tag{2.24}$$

The first four terms on the right-hand side can be evaluated using various vector calculus identities, resulting in

$$\begin{aligned}
\nabla\psi\cdot\nabla(\nabla\varphi) &= -\left(\frac{\partial\psi}{\partial R}\hat{R} + \frac{\partial\psi}{\partial Z}\hat{Z}\right)\cdot\nabla\left(\frac{\hat{\varphi}}{R}\right) = \frac{\hat{\varphi}}{R^2}\frac{\partial\psi}{\partial R}\\
\nabla\varphi\cdot\nabla(\nabla\psi) &= \frac{\hat{\varphi}}{R}\cdot\nabla\left(\frac{\partial\psi}{\partial R}\hat{R} + \frac{\partial\psi}{\partial Z}\hat{Z}\right) = \frac{\partial\psi}{\partial R}\frac{\hat{\varphi}}{R^2}\\
-\nabla\varphi(\nabla\cdot\nabla\psi) &= -\frac{\hat{\varphi}}{R}\left[\frac{1}{R}\frac{\partial}{\partial R}\left(R\frac{\partial\psi}{\partial R}\right) + \frac{\partial^2\psi}{\partial Z^2}\right]\\
\nabla\psi(\nabla\cdot\nabla\varphi) &= \nabla\psi\left[\frac{1}{R}\frac{\partial}{\partial\varphi}\left(\frac{1}{R}\right)\right] = 0.
\end{aligned} \tag{2.25}$$

Thus, $\nabla \times \vec{B}$ becomes

$$\begin{aligned}\nabla \times \vec{B} &= \frac{\hat{\varphi}}{R^2}\frac{\partial \psi}{\partial R} + \frac{\partial \psi}{\partial R}\frac{\hat{\varphi}}{R^2} - \frac{\hat{\varphi}}{R}\left[\frac{1}{R}\frac{\partial}{\partial R}\left(R\frac{\partial \psi}{\partial R}\right) + \frac{\partial^2 \psi}{\partial Z^2}\right] + \frac{\mathrm{d}F}{\mathrm{d}\psi}\nabla\psi \times \nabla\varphi \\ &= -\frac{\hat{\varphi}}{R}\left(\frac{\partial^2}{\partial R^2} - \frac{1}{R}\frac{\partial}{\partial R} + \frac{\partial^2}{\partial Z^2}\right)\psi + \frac{\mathrm{d}F}{\mathrm{d}\psi}\nabla\psi \times \nabla\varphi \\ &= -\frac{\hat{\varphi}}{R}\Delta^*\psi + \frac{\mathrm{d}F}{\mathrm{d}\psi}\nabla\psi \times \nabla\varphi,\end{aligned} \tag{2.26}$$

where Δ^* is the Grad-Shafranov operator[3]. Plugging Eqs. 2.23 and 2.26 into Eq. 2.18 yields

$$\begin{aligned}0 &= -\nabla p + \frac{1}{\mu_0}\left[-\frac{\hat{\varphi}}{R}\Delta^*\psi + \frac{\mathrm{d}F}{\mathrm{d}\psi}\nabla\psi \times \nabla\varphi\right] \times [\nabla\psi \times \nabla\varphi + F\nabla\varphi] \\ &= -\frac{\mathrm{d}p}{\mathrm{d}\psi}\nabla\psi + \left(\frac{\Delta^*\psi}{\mu_0} + \frac{F}{\mu_0}\frac{\mathrm{d}F}{\mathrm{d}\psi}\right)(\nabla\psi \times \nabla\varphi) \times \nabla\varphi \\ &= -\nabla\psi\left(\frac{\mathrm{d}p}{\mathrm{d}\psi} + \frac{\Delta^*\psi}{\mu_0 R^2} + \frac{F}{\mu_0 R^2}\frac{\mathrm{d}F}{\mathrm{d}\psi}\right).\end{aligned} \tag{2.27}$$

After a bit of rearranging, the Grad-Shafranov equation in SI units is

$$\Delta^*\psi = -\mu_0 R^2\frac{\mathrm{d}p}{\mathrm{d}\psi} - F\frac{\mathrm{d}F}{\mathrm{d}\psi}. \tag{2.28}$$

The functions $p(\psi)$ and $F(\psi)$ are free functions, meaning that the Grad-Shafranov equation can be solved for an arbitrary choice of $p(\psi)$ and $F(\psi)$. Moreover, alternative free functions which then determine $p(\psi)$ and $F(\psi)$ could be defined. At the outset, however, $p(\psi)$ and $F(\psi)$ must be defined.

2.3 The Shafranov Shift

The Shafranov shift is an outward shift of the nested surfaces of constant ψ. Analytical solutions are typically found in the limit of large aspect ratio, and when the safety factor $q \sim 1$ [8]. Let's first imagine a coordinate system that is centered about the outer-most flux surface of the plasma, and that each flux surface is circular. The direction perpendicular to

[3]A general 2D elliptic operator in cylindrical coordinates can be written as $R^{-m}\frac{\partial}{\partial R}(R^m\frac{\partial}{\partial R}) + \frac{\partial^2}{\partial Z^2}$. For the Laplacian, $m = 1$, for the Grad-Shafranov operator, $m = -1$.

the surfaces is $\hat{r}$, the direction tangent to the flux surface is $\hat{\theta}$, then $\hat{\phi} = \hat{r} \times \hat{\theta}$, which is the azimuthal direction. The quantities, $r,\ \theta,\ \phi$, relate to the original cylindrical coordinates by

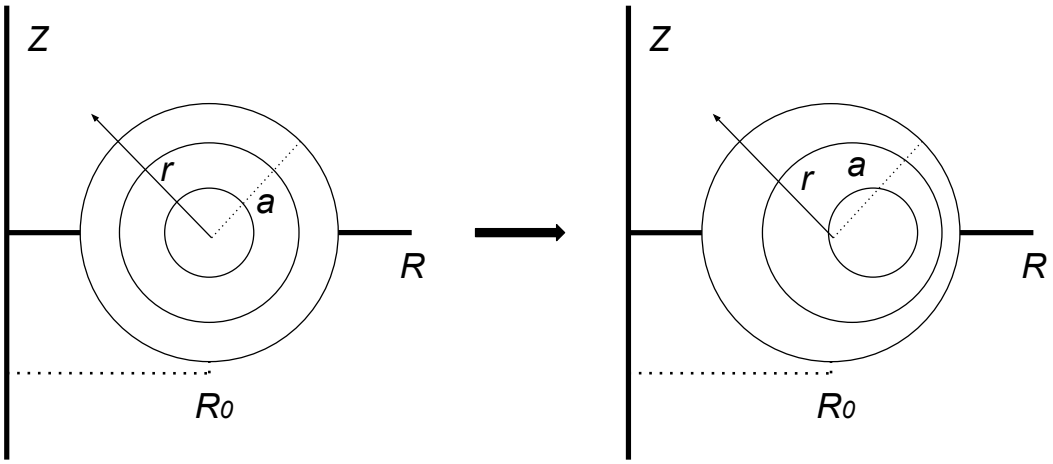

Figure 2.1: A diagram of how the flux surfaces of constant ψ are shifted outward as a result of the Shafranov shift. Note that $\vec{r}$, a, and R_0 are from the center of the outermost flux surface, and not necessarily from the magnetic axis.

$$\begin{aligned} r &= \sqrt{(R - R_0)^2 + Z^2} \\ \theta &= \arctan \frac{Z}{R - R_0} \\ \phi &= -R_0 \varphi. \end{aligned} \tag{2.29}$$

A helpful diagram for visualizing the new coordinates and the Shafranov shift is shown in Fig. 2.1. After some algebra, the Grad-Shafranov operator in this new coordinate system is [8]

$$\Delta^* \psi = \underbrace{\frac{1}{r}\frac{\partial}{\partial r}\left(r\frac{\partial \psi}{\partial r}\right) + \frac{1}{r^2}\frac{\partial^2}{\partial \theta^2}}_{\nabla_c^2} + \frac{1}{R}\left(\cos\frac{\partial \psi}{\partial r} - \frac{\sin\theta}{r}\frac{\partial \psi}{\partial \theta}\right), \tag{2.30}$$

$$\nabla_c^2 \psi = \mu_0 R^2 \frac{\mathrm{d}p}{\mathrm{d}\psi} - \frac{1}{2}\frac{\mathrm{d}F^2}{\mathrm{d}\psi} + \frac{1}{R}\left(\cos\frac{\partial \psi}{\partial r} - \frac{\sin\theta}{r}\frac{\partial \psi}{\partial \theta}\right). \tag{2.31}$$

In this particular case, we assume that the inverse aspect ratio, $\epsilon = a/R_0$, is much less than 1. We also require that the poloidal plasma pressure, $\beta_\mathrm{p} = 2\mu_0 p / B_\mathrm{p}^2 \sim 1$ [8]. We define

$G(\psi)$ via the equation

$$F^2(\psi) = R_0^2 B_0^2 + G(\psi), \tag{2.32}$$

and expand ψ in powers of ϵ,

$$\psi(r,\theta) = \psi_0(r,\theta) + \psi_1(r,\theta) + ..., \tag{2.33}$$

where the powers of ϵ are absorbed into ψ_n, so that $\psi_{n+1} << \psi_n$. A Taylor expansion then yields

$$\begin{aligned} \frac{\mathrm{d}p}{\mathrm{d}\psi} &= \frac{\mathrm{d}p}{\mathrm{d}\psi}(\psi_0) + \psi_1 \frac{\mathrm{d}^2 p}{\mathrm{d}\psi^2}(\psi_0) + ... \\ \frac{\mathrm{d}F^2}{\mathrm{d}\psi} &= \frac{\mathrm{d}F^2}{\mathrm{d}\psi}(\psi_0) + \psi_1 \frac{\mathrm{d}^2 F^2}{\mathrm{d}\psi^2}(\psi_0) + ... \,. \end{aligned} \tag{2.34}$$

Substituting Eqs. 2.32 and 2.34 into Eq. 2.31 yields,

$$\begin{aligned} \nabla_c^2\psi_0 + \nabla_c^2\psi_1 + ... = -\mu_0 \left(R_0^2 + 2\pi R_0 \cos\theta + ...\right) \left[\frac{\mathrm{d}p}{\mathrm{d}\psi}(\psi_0) + \psi_1 \frac{\mathrm{d}^2 p}{\mathrm{d}\psi^2}(\psi_0) + ...\right] \\ - \frac{1}{2}\frac{\mathrm{d}F^2}{\mathrm{d}\psi}(\psi_0) + \frac{\psi_1}{2}\frac{\mathrm{d}^2 F^2}{\mathrm{d}\psi^2}(\psi_0) + \frac{1}{R_0}\left(\cos\theta \frac{\partial\psi_0}{\partial r} - \frac{\sin\theta}{r}\frac{\partial\psi}{\partial\theta}\right) + ... \,. \end{aligned} \tag{2.35}$$

Looking at the zeroth order terms, ψ_0, the desired solutions are $\psi_0(r,\theta) = \psi_0(r)$, as at this order the boundary conditions are independent of θ. The zeroth order equation simplifies to

$$\frac{1}{r}\frac{\partial}{\partial r}\left(r\frac{\partial\psi_0}{\partial r}\right) = -\mu_0 R_0^2 \frac{\mathrm{d}p}{\mathrm{d}\psi}(\psi_0) - \frac{1}{2}\frac{\mathrm{d}F^2}{\mathrm{d}\psi}(\psi_0). \tag{2.36}$$

Rewriting this to fit the force balance of a screw pinch results in

$$\begin{aligned} B_{r0}(r) &= 0 \\ B_{\theta 0}(r) &= \frac{1}{R_0}\frac{\partial\psi}{\partial r} \\ B_{z0}(r) &= -\frac{F(\psi_0)}{R_0} \\ p_0(r) &= p(\psi_0). \end{aligned} \tag{2.37}$$

Eq. 6.62 in Freidberg's *Ideal MHD* gives the force balance for a screw pinch as,

$$0 = \frac{\mathrm{d}}{\mathrm{d}r}\left[\mu_0 p_0 + \frac{1}{2}\left(B_\theta^2 + B_z^2\right)\right] - \frac{B_\theta^2}{r}. \tag{2.38}$$

Instead of specifying the free functions as $p(\psi_0)$ and $F(\psi_0)$, the free functions can be expressed as $p(r)$ and $B_{\theta 0}(r)$. $p(\psi_0)$ can be readily solved for once ψ_0 is found from the integral,

$$\psi_0 = \int_0^r R_0 B_{\theta 0}(r')\,\mathrm{d}r'. \tag{2.39}$$

Solving Eq. 2.38 then determines $B_{z0}(r)$, which determines $F(\psi_0)$ via

$$F(\psi_0) = -R_0 B_{z0}(r(\psi_0)). \tag{2.40}$$

For the first order terms, the Grad-Shafranov equation looks like

$$\nabla_c^2\psi_1 + \psi_1\left[\mu_0 R_0^2 \frac{\mathrm{d}^2 p}{\mathrm{d}\psi^2}(\psi_0) + \frac{1}{2}\frac{\mathrm{d}F^2}{\mathrm{d}\psi}(\psi_0)\right] = \left[\frac{1}{R_0}\frac{\mathrm{d}\psi_0}{\mathrm{d}r} - 2\mu_0\frac{\mathrm{d}p}{\mathrm{d}\psi}(\psi_0)R_0 r\right]\cos\theta. \tag{2.41}$$

Here, the desired form of ψ_1 is $\psi_1(r,\theta) = \bar{\psi}_1(r)\cos\theta$. After some algebra, $\bar{\psi}_1(r)$ can be expressed as

$$\bar{\psi}_1(r) = B_{\theta 0}(r)\int_a^r \frac{1}{B_{\theta 0}^2(x)}\int_0^x \left[yB_{\theta 0}^2(y) - 2\mu_0 y^2\frac{\mathrm{d}p_0}{\mathrm{d}r}(y)\right]\,\mathrm{d}y\,\mathrm{d}x. \tag{2.42}$$

Finally, with $\bar{\psi}_1(r)$, the shift of the flux surface of radius r can be found via [8]

$$\Delta(r) = -\frac{\bar{\psi}_1(r)}{R_0 B_{\theta 0}(r)}. \tag{2.43}$$

CHAPTER 3

The Grad-Shafranov Computational Solver

The code I wrote is a successive over-relaxation free-boundary Grad-Shafranov equation solver. In this chapter, I will first discuss the successive over-relaxation aspect of the code, then I will discuss the modifications necessary to turn a simple successive over-relaxation code into a free-boundary Grad-Shafranov equation solver.

3.1 Succcessive Over-relaxation

To solve the Grad-Shafranov equation, it's useful to define a discretized grid in R and Z made up of $N_R \times N_Z$ points. Each point is then labeled with a pair of indices, i, j, where each index ranges from 0 to $N-1$, or n. A visualization of the discretized grid is shown in Fig. 3.1. On a discretized grid like this, derivatives can be written in terms of finite differences. In the case of the Grad-Shafranov equation (Eq. 2.28), the discretized form to second-order looks like [11]

$$\frac{R_i}{(\Delta R)^2 R_{i+1/2}}\psi_{i+1,\,j} - \left[\frac{R_i}{(\Delta R)^2 R_{i+1/2}} + \frac{R_i}{(\Delta R)^2 R_{i-1/2}} + \frac{2}{(\Delta Z)^2}\right]\psi_{i,\,j} + \frac{R_i}{(\Delta R)^2 R_{i-1/2}}\psi_{i-1,\,j} + \frac{1}{(\Delta Z)^2}\psi_{i,\,j+1} + \frac{1}{(\Delta Z)^2}\psi_{i,\,j-1} = S_{i,\,j}, \quad (3.1)$$

where the RHS has been rewritten as a source function, S, for simplicity, and ΔR and ΔZ are the step sizes in R and Z. As an aside that will be relevant later in the chapter, the

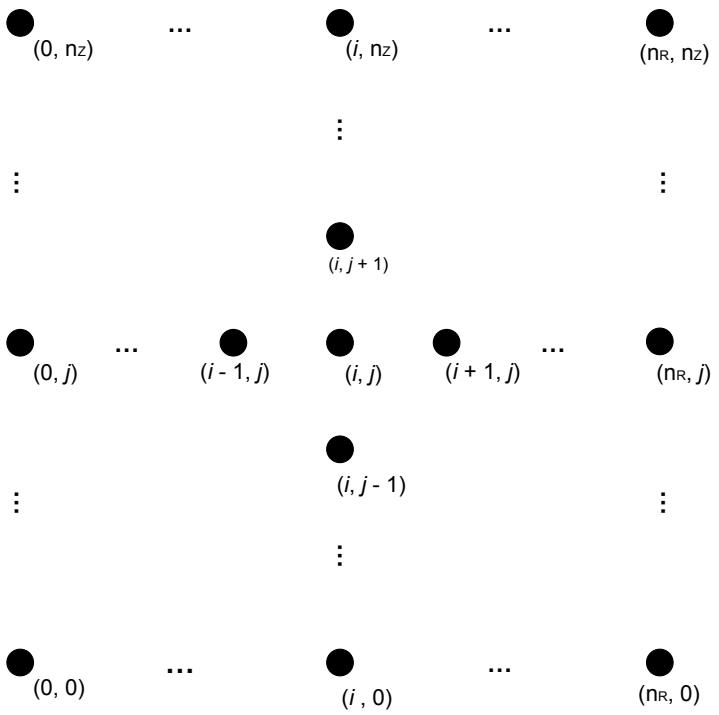

Figure 3.1: A visualization of the computational domain.

RHS of Eq. 2.28 can be written in terms of a toroidal current density, J_φ [8, 11],

$$-\mu_0 R^2 \frac{\mathrm{d}p}{\mathrm{d}\psi} - F\frac{\mathrm{d}F}{\mathrm{d}\psi} = \mu_0 R J_\varphi. \tag{3.2}$$

To simplify the notation of Eq. 3.1 the following substitutions are made [12],

$$\begin{aligned}
E_i &= -\left[\frac{R_i}{(\Delta R)^2 R_{i+1/2}} + \frac{R_i}{(\Delta R)^2 R_{i-1/2}} + \frac{2}{(\Delta Z)^2}\right] \\
A_i &= \frac{R_i}{(\Delta R)^2 R_{i+1/2}}\frac{1}{E_i} \\
B_i &= \frac{R_i}{(\Delta R)^2 R_{i-1/2}}\frac{1}{E_i} \\
C_i &= \frac{1}{(\Delta Z)^2}\frac{1}{E_i} \\
D_i &= \frac{1}{(\Delta Z)^2}\frac{1}{E_i} \\
\delta_i &= \frac{1}{E_i}.
\end{aligned} \tag{3.3}$$

Plugging Eq. 3.3 into Eq. 3.1 and rearranging yields,

$$\psi_{i,\,j} = \delta_i S_{i,\,j} - A_i \psi_{i+1,\,j} - B_i \psi_{i-1,\,j} - C_i \psi_{i,\,j+1} - D_i \psi_{i,\,j-1}. \tag{3.4}$$

Now that the equation has been sufficiently simplified, it is time to actually solve for ψ. One method for solving is called successive over-relaxation, where the first approximation of a solution is used to calculate the second approximation, which is used to calculate the third, etc., until convergence is reached. Modifying Eq. 3.4 for a successive over-relaxation method yields [12],

$$\psi_{i,\,j}^{k+1} = (1 - \omega_{\text{opt}})\psi_{i,\,j}^{k} + \omega_{\text{opt}}(\delta_i S_{i,\,j} - A_i \psi_{i+1,\,j}^{k} - B_i \psi_{i-1,\,j}^{k+1} - C_i \psi_{i,\,j+1}^{k} - D_i \psi_{i,\,j-1}^{k+1}), \tag{3.5}$$

where k is how many iterations have happened, and ω_{opt} is the over-relaxation factor. The over-relaxation factor depends on the characteristics of the mesh grid via,

$$\omega_{\text{opt}} = 2\left(\frac{1 - \sqrt{1 - \xi}}{\xi}\right), \tag{3.6}$$

where

$$\xi = \left[\frac{\cos\left(\frac{\pi}{n_R}\right) + \beta^2 \cos\left(\frac{\pi}{n_Z}\right)}{1 + \beta^2}\right]^2, \tag{3.7}$$

where $\beta = \Delta R / \Delta Z$. Convergence is determined by a weighted root-mean-square [12],

$$\left[\frac{1}{n_R n_Z} \sum \left(W_{i,\,j} |\psi_{i,\,j}^{k+1} - \psi_{i,\,j}^{k}|\right)^2\right]^{1/2} < 1, \tag{3.8}$$

where the weights, $W_{i,\,j}$, are

$$W_{i,\,j} = \frac{1}{\text{RT}|\psi_{i,\,j}^{k+1}| + \text{AT}}. \tag{3.9}$$

The relative tolerance, RT, and absolute tolerance, AT, can be specified.

3.2 The Free-Boundary Loop

To model complex tokamak geometries with additional shaping coils and solenoids, a free-boundary solver is one of the more straightforward approaches [11, 13]. There are three important parts to turning the successive over-relaxation code into a free-boundary solver. First, critical point analysis must be done to determine where the magnetic axis is, and where the limiter and saddle points are in relation to the magnetic axis to define the plasma boundary [11]. Next, $p(\psi)$ and $F(\psi)$ must be written in terms of a normalized ψ inside of the plasma to recalculate the plasma current density, J_φ [13]. Lastly, the contribution of J_φ and other shaping coils must be calculated on the computational boundary before calling the successive over-relaxation routine. The following subsections provide a bit more detail on each of these steps.

3.2.1 Critical Point Analysis

For this code, the only critical points of interest are saddle points, if they exist, and minima. The best way to determine where these points are is through partial differentiation. To find a local minimum, there are a couple of criteria that the partial derivatives need to satisfy at a given point. For this subsection, a subscript R or Z on ψ is used to denote differentiation of ψ with respect to R or Z. The criteria needed for finding the local minimum (also called the magnetic axis) is [11]

$$\psi_R = \psi_Z = 0,\ \psi_{RR} > 0,\ \text{and } D > 0,$$

where,

$$D = \psi_{RR}\psi_{ZZ} - \psi_{RZ}^2.$$

For a saddle point, the criteria is [11],

$$\psi_R = \psi_Z = 0, \text{ and } D < 0.$$

The easiest way to calculate these partial derivatives is via a second order finite difference method.

It is also important to implement a limiter, in the event that there are no saddle points within the computational domain. With a limiter specified, it must be determined if the saddle point or the limiter is closer to the magnetic axis, which can be done via the distance formula,

$$d = \sqrt{(R_2 - R_1)^2 + (Z_2 - Z_1)^2}. \tag{3.10}$$

After determining which is closer to the magnetic axis, the lowest valued contour of ψ that touches the saddle point or limiter is used to define the plasma boundary.

3.2.2 Normalizing ψ and updating J_φ

To determine J_φ, a normalized poloidal flux function, $\tilde{\psi}$, is defined as [11, 13, 14],

$$\tilde{\psi} = \frac{\psi_{\text{edge}} - \psi}{\psi_{\text{edge}} - \psi_{\text{min}}}. \tag{3.11}$$

This $\tilde{\psi}$ ranges in value from 1 at the magnetic axis to 0 at the plasma edge. The free functions, $p(\psi)$ and $\frac{1}{2}F^2(\psi)$, can be defined in terms of $\tilde{\psi}$ via,

$$\begin{aligned} p(\psi) &= p_0 \hat{p}(\tilde{\psi}) \\ \frac{1}{2}F^2(\psi) &= \frac{1}{2}F_0^2[1 + \alpha_g \hat{F}(\tilde{\psi})], \end{aligned} \tag{3.12}$$

where p_0 is the pressure on the magnetic axis and F_0 is the vacuum value of the toroidal field function. $\hat{p}$ and $\hat{F}$ are defined as

$$\begin{aligned} \hat{p} &= \tilde{\psi}^{n_1} \\ \hat{F} &= \tilde{\psi}^{n_2}, \end{aligned} \tag{3.13}$$

where n_1 and n_2 are positive valued numbers that control the peakedness of p and F. To determine α_g, a total plasma current, I, is specified to be fixed from iteration to iteration. I can be related to the current density via,

$$I = \sum_{i,\,j} J_{\varphi\,i,\,j} \Delta R \Delta Z. \tag{3.14}$$

Some re-arranging of Eq. 3.2 gives,

$$J_\varphi = -R\frac{\mathrm{d}p}{\mathrm{d}\psi} - \frac{1}{2\mu_0 R}\frac{\mathrm{d}F^2}{\mathrm{d}\psi}. \tag{3.15}$$

The discretized form of J_φ in terms of Eq. 3.12 is,

$$J_{\varphi\,i,\,j} = -\frac{R_i p_0}{\Delta\psi}\hat{p}'(\tilde{\psi}_{i,\,j}) - \frac{F_0^2\alpha_g}{2\mu_0 R_i \Delta\psi}\hat{F}'(\tilde{\psi}_{i,\,j}). \tag{3.16}$$

Plugging Eq. 3.16 into Eq. 3.14 yields,

$$I = \sum_{i,\,j}\left[-\frac{R_i p_0}{\Delta\psi}\hat{p}'(\tilde{\psi}_{i,\,j}) - \frac{F_0^2\alpha_g}{2\mu_0 R_i \Delta\psi}\hat{F}'(\tilde{\psi}_{i,\,j})\right]\Delta R \Delta Z, \tag{3.17}$$

where $\Delta\psi = \psi_{\mathrm{edge}} - \psi_{\mathrm{min}}$. With some rearranging of Eq. 3.17 and keeping I constant, α_g is then,

$$\alpha_g = -\mu_0\left[\frac{p_0 R_i \sum_{i,\,j}\hat{p}'(\tilde{\psi}_{i,\,j}) + I\Delta\psi/(\Delta R\Delta Z)}{\frac{1}{2}F_0^2\sum_{i,\,j}\hat{F}'(\tilde{\psi}_{i,\,j})/R_i}\right]. \tag{3.18}$$

To summarize the subsection, p_0 is the pressure on the magnetic axis and F_0 is the fixed vacuum value of the toriodal field function. Updating the current density, J_φ, is done by

first normalizing ψ via Eq. 3.11 and calculating $\hat{p}'(\tilde{\psi})$ and $\hat{F}'(\tilde{\psi})$. Those functions are then plugged into Eq. 3.18 to determine α_g such that I is constant between iterations. J_φ is then calculated via Eq. 3.16, which then is used in part for the source, S, for the next successive over-relaxation loop.

3.2.3 Determining ψ on the Computational Boundary

Determining ψ on the computational boundary is the final step before calling the successive over-relaxation code again. To do this, the Green's function of an axisymmetric current source is used [15],

$$G(R, R'; Z, Z') = \frac{\mu_0 \sqrt{RR'}}{2\pi k} \left[(2 - k^2)K(k) - 2E(k) \right], \tag{3.19}$$

where

$$k^2 = \frac{4RR'}{(R + R')^2 + (Z - Z')^2}, \tag{3.20}$$

and $K(k)$ and $E(k)$ are the complete elliptic integrals of the first and second kind, respectively. Obtaining the contribution from the coils is straightforward,

$$\psi_{\text{coils}} = \sum_{c=1}^{N} G(R, R'_c; Z, Z'_c) I_c, \tag{3.21}$$

where N is the total number of external coils and R'_c, Z'_c, and I_c correspond the to position and current of coil, c. This contribution only has to be calculated once at the beginning [11, 13]. Between calls of the successive over-relaxation routine, the contribution from the plasma on the boundary is calculated as,

$$\psi_{\text{plasma}} = \sum_{i,\,j} G(R, R'_i; Z, Z'_j) J_{\varphi\, i,\, j} \Delta R \Delta Z. \tag{3.22}$$

In full, the boundary values of ψ are,

$$\psi_{\text{boundary}} = \psi_{\text{plasma}} + \psi_{\text{coils}} = \sum_{i,\,j} G(R, R_i'; Z, Z_j') J_{\varphi\, i,\, j} \Delta R \Delta Z + \sum_{c=1}^{N} G(R, R_c'; Z, Z_c') I_c. \quad (3.23)$$

A helpful visualization of the nested loop structure of the code is shown in Fig. 3.2. The outer loop houses all of the routines for determining the plasma boundary, J_φ, and ψ in the computational boundary. The inner loop is the successive over-relaxation routine from

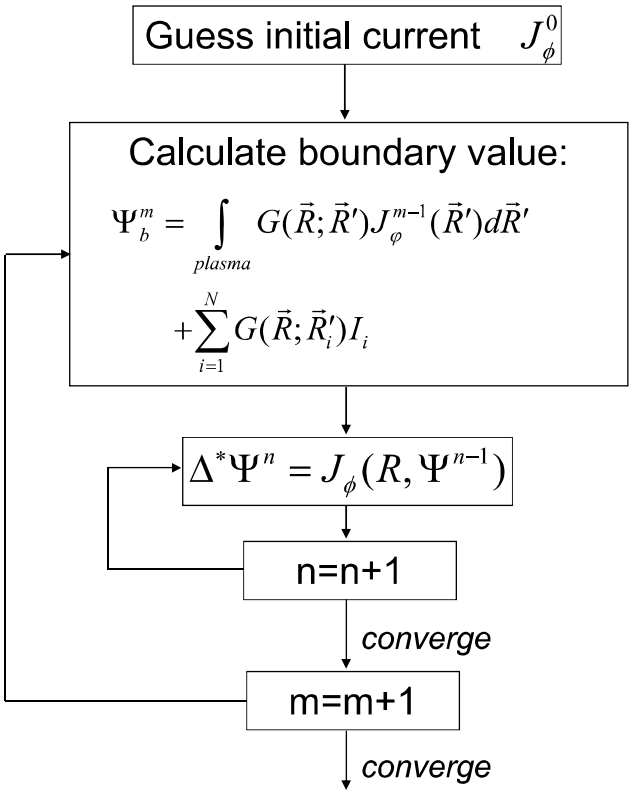

Figure 3.2: From Jardin as Fig. 4.8. A flowchart of the free-boundary code. The inner loop is the successive over-relaxation routine covered in Section 3.1. The outer loop contains all of the routines to determine the plasma edge, J_φ, and ψ on the computational boundary.

Section 3.1. Convergence of the outer loop occurs when the difference between successive iterations of boundary values falls within a desired tolerance.

CHAPTER 4

Results

This chapter covers comparison with analytical solutions. The tests are focused on the successive over-relaxation routine. The first comparison is with a Solov'ev solution from López et al. (2019) to see how well the successive over-relaxation routine can calculate a single analytical plasma equilibrium. The second comparison is of the Shafranov shift. The equations of $B_{\theta 0}$ and p were chosen such that the RHS of the Grad-Shafranov equation are constant as a increases. This test ensures that variation in the values of ψ on the boundary are accurately represented throughout the computational domain. Lastly, a plasma equilibrium in a simple tokamak is presented using the free-boundary loop.

4.1 Solov'ev Comparison

The Solov'ev solution is one of the simplest, non-trivial, non-vacuum solutions to the Grad-Shafranov equation. The form of the equation used in this comparison is [14],

$$\psi(R, Z) = \frac{1}{2}(c_2 R_0^2 + c_0 R^2)Z^2 + \frac{1}{8}(c_1 - c_0)(R^2 - R_0^2)^2, \tag{4.1}$$

where $c_0,\ c_1$ andc_2 are constants. The various constants are then defined as,

$$\begin{aligned} c_0 &= \frac{B_0}{R_0^2 \kappa_0 q_0} \\ c_1 &= \frac{B_0(\kappa_0^2 + 1)}{R_0^2 \kappa_0 q_0} \\ c_2 &= 0. \end{aligned} \tag{4.2}$$

The values for the constants can be found in Table 4.1. With this choice of coefficients, the

Table 4.1: Values of the constants defined in Lopez et al. [14].

constant	value
B_0	0.5 T
R_0	.95 m
κ_0	2.2
q_0	1.1

free functions are written as,

$$\begin{aligned} \frac{\mathrm{d}p}{\mathrm{d}\psi} &= -\frac{c_1}{\mu_0} \\ F\frac{\mathrm{d}F}{\mathrm{d}\psi} &= -R_0^2 c_2 = 0. \end{aligned} \tag{4.3}$$

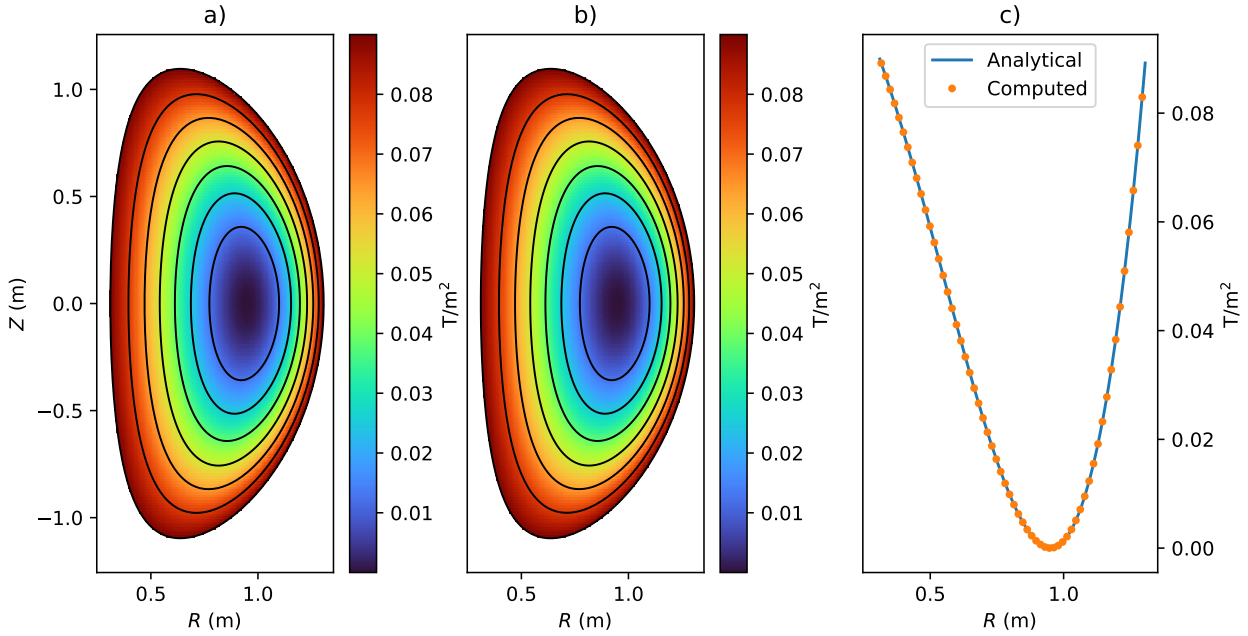

Figure 4.1: A recreation of Fig. 4 in López et al. (2019). A comparison of analytical and computational Solov'ev solutions. Subplot a) shows the analytical solution, subplot b) shows the computational solution, and subplot c) shows a comparison between the computational and analytical solutions on the line $Z = 0$. For these plots, $n_r = n_z = 199$, RT $= 1 \times 10^{-7}$, AT $= 1 \times 10^{-6}$.

The resulting analytical and computational solutions are shown in Fig. 4.1. Subplots a) and b) show good agreement upon visual inspection. Subplot c) shows a direct comparison between the numerical solution and the analytical solution on the line $Z = 0$.

4.2 Shafranov Shift Comparison

Recalling the derivations from Section 2.3, the free functions that are specified are $B_{\theta 0}(r)$ and $p(r)$. The forms of these functions in this comparison are

$$\begin{aligned} B_{\theta 0}(r) &= \frac{c_1}{R_0} r \\ p(r) &= c_3 - c_2 r^2, \end{aligned} \tag{4.4}$$

where c_1, c_2, and c_3 are arbitrary constants. Integrating $B_{\theta 0}(r)$ with respect to r in Eq. 2.39 yields the zeroth order term in the expansion of ψ,

$$\psi_0(r) = \frac{c_1}{2} r^2. \tag{4.5}$$

Later, it will be useful to have r as a function of ψ_0,

$$r(\psi_0) = \sqrt{\frac{2\psi_0}{c_1}}. \tag{4.6}$$

Substituting $p(r)$ and $B_{\theta 0}(r)$ into Eq. 2.38 and solving for B_{z0} yields,

$$B_{z0}(r) = \sqrt{\frac{-2c_1^2}{R_0^2} r^2 + 2c_3 + 2\mu_0 c_2 r^2}. \tag{4.7}$$

Making the proper substitutions, then squaring and halving Eq. 2.40 yields,

$$\frac{1}{2} F^2(\psi_0) = -2c_1\psi_0 + R_0^2 c_3 + \frac{2\mu_0 c_2 R_0^2 \psi_0}{c_1} \tag{4.8}$$

The pressure in terms of ψ_0 is,

$$p(\psi_0) = c_3 - \frac{2c_2}{c+1}\psi_0. \tag{4.9}$$

The derivatives with respect to ψ_0 of Eqs. 4.8 and 4.9 are then,

$$\begin{aligned} \frac{\mathrm{d}}{\mathrm{d}\psi_0}\left[\frac{1}{2}F^2(\psi_0)\right] &= -2c_1 + \frac{2\mu_0 c_2 R_0^2}{c_1} \\ \frac{\mathrm{d}}{\mathrm{d}\psi_0}[p(\psi_0)] &= -\frac{2c_2}{c_1}. \end{aligned} \tag{4.10}$$

This makes the RHS of the Grad-Shafranov equation to zeroth order,

$$-\frac{\mathrm{d}}{\mathrm{d}\psi_0}\left[\frac{1}{2}F^2(\psi_0) + p(\psi_0)\right] = \frac{2c_2}{c_1} + 2c_1 - \frac{2\mu_0 c_2 R_0^2}{c_1}. \tag{4.11}$$

By a convenient choice of B_{z0} and p, the only non-zero term in the RHS of Eq. 2.34 is the zeroth order term, meaning that the source function in the successive over-relaxation routine will remain constant as any free parameter in $\bar{\psi}_1$ varies. $\bar{\psi}_1$ in this comparison is,

$$\bar{\psi}_1(r) = \left\{\frac{c_1 r}{R_0}\left[\frac{1}{3}(r-a) + \frac{\mu_0 R_0^2 c_2}{2c_1^2}(r^2 - a^2)\right]\right\}, \tag{4.12}$$

where a is the minor radius of the plasma, but also acts as a free parameter. Recalling Eq. 2.43,

$$\Delta(r) = -\frac{\bar{\psi}_1(r)}{R_0 B_{\theta 0}(r)},$$

the Shafranov shift increases as a increases. It is easiest to measure the shift of the magnetic axis at $r = 0$, as it is a local minimum. The values of ψ on the computational boundary are analytical,

$$\psi(r,\theta) = \psi_0(r) + \bar{\psi}_1(r)\cos\theta = \frac{c_1}{2}r^2 + \left\{\frac{c_1 r}{R_0}\left[\frac{1}{3}(r-a) + \frac{\mu_0 R_0^2 c_2}{2c_1^2}(r^2 - a^2)\right]\right\}\cos\theta. \tag{4.13}$$

The last constants that need to be defined are $c_1 = .22$, $c_2 = 15$, and $R_0 = 100$ m.

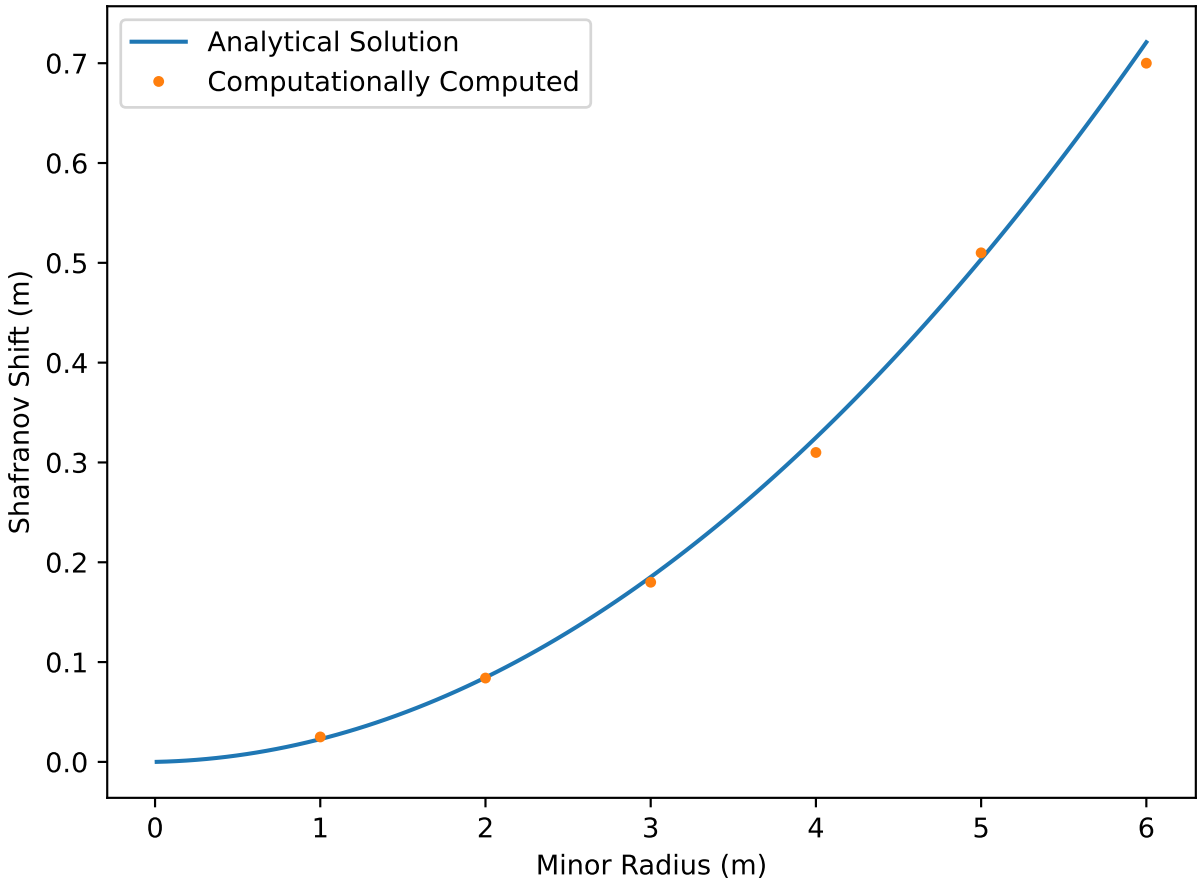

Figure 4.2: A plot of Shafranov shift as a function of minor radius. The analytical solution for the Shafranov shift is shown by the blue line and the computational solutions are shown as the orange dots.

Fig. 4.2 shows the analytical Shafranov shift and the numerical values of the shift using successive over-relaxation. For minor radii between 1 m and 6 m, the two show good agreement. These radii correspond to a range of aspect ratios that spans from 100 to 16.67, which lies within the asymptotic limit of large aspect ratio.

4.3 Equilibrium in a Simple Tokamak

For a simple, realistic tokamak, an ohmic heating solenoid and two poloidal field coils are added outside of the computational domain. The solenoid is positioned at $R = 1$, spans from $Z = -2$ to $Z = 2$, and has 100 turns. The poloidal field coils are positioned at $R = 5$

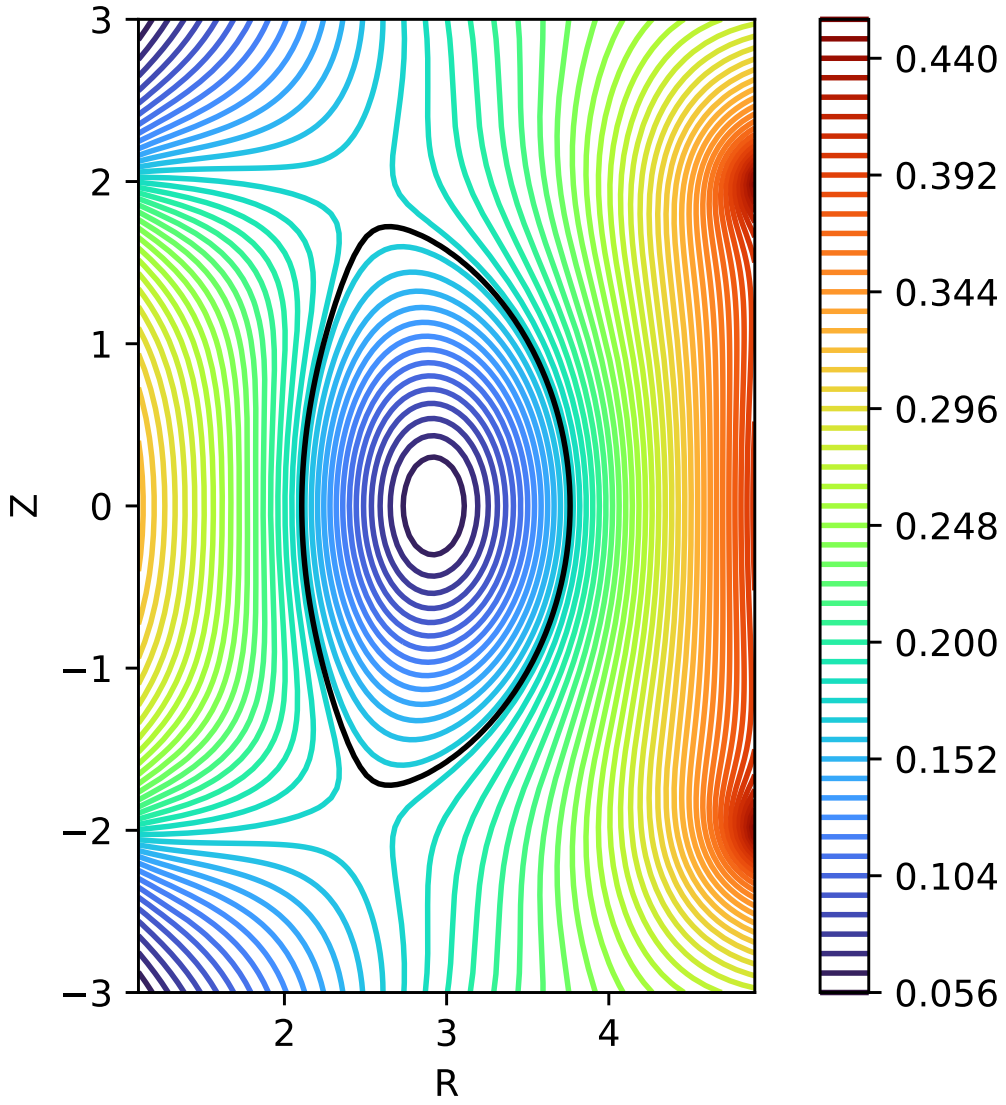

Figure 4.3: A free-boundary plasma equilibrium in a simple tokamak.

and $Z = \pm 2$. The solenoid has 20,000 A of current, while the two field coils have 50,000 A. The total plasma current, I, is set to 300,000 A. Other important constants are $p_0 = 2000$ Pa, and $F_0 = .4$ T·m. Fig. 4.3 shows the resulting plasma equilibrium from this simple tokamak.

CHAPTER 5

Concluding Remarks

In this work, I have shown how successive over-relaxation can be used to code a free-boundary Grad-Shafranov equation solver. Most of the results in Chapter 4 are focused on testing the successive over-relaxation routine to ensure it can reproduce analytical solutions. Testing the entire free-boundary loop is a bit more challenging, as the various coils and solenoids contribute to B_{T} and B_{p}, which can cause significant deviation from an analytical solution. Future work on this topic would involve devising a coil arrangement that agrees well with analytical solutions to test the entire free-boundary loop. Ultimately, this tool serves as a good starting point for testing plasma equilibria for a given coil and solenoid configuration in the early design phase of tokamaks.

Bibliography

[1] R. D. Knight, *Physics for Scientists and Engineers*, 4th (Pearson, 2017).

[2] D. G. Griffiths, *Introduction to Electrodynamics*, 4th (Pearson, 2013).

[3] M.-B. Kallenrode, *Space Physics* (Springer-Verlag Berlin Heidelberg, 2004).

[4] J. L. Shohet, *The Plasma State* (Academic Press, 1971).

[5] W. Baumjohann and R. A. Treumann, *Basic Space Plasma Physics* (Imperial College Press, 2012).

[6] L. Euler, "Principia motus fluidorum", Novi Commentarii Academiae Scientiarum Imperialis Petropolitanae **6**, 271–311 (1761).

[7] L. Landau and E. Lifshitz, *Fluid Mechanics*, 2nd ed., Vol. 6 (Pergamon Press, 1987).

[8] J. P. Freidberg, *Ideal MHD* (Cambridge University Press, 2014).

[9] H. Grad and H. Rubin, "Hydromagnetic equilibria and force-free fields", Journal of Nuclear Energy **7**, 284–285 (1958).

[10] V. D. Shafranov, "Plasma Equilibrium in a Magnetic Field", Reviews of Plasma Physics **2**, 103 (1966).

[11] S. Jardin, *Computational Methods in Plasma Physics* (CRC Press, 2010).

[12] M. A. Salem, "Numerical solution of poisson's equation in cylindrical coordinates using finite difference method", Florida Institute of Technology (2013).

[13] J. Johnson, H. Dalhed, J. Greene, R. Grimm, Y. Hsieh, S. Jardin, J. Manickam, M. Okabayashi, R. Storer, A. Todd, D. Voss, and K. Weimer, "Numerical determination of axisymmetric toroidal magnetohydrodynamic equilibria", Journal of Computational Physics **32**, 212–234 (1979).

[14] J. E. López, E. A. Orozco, and V. D. Dougar-Zhabon, "Fixed boundary grad-shafranov solver using finite difference method in nonhomogeneous meshgrid", Journal of Physics: Conference Series **1159**, 10.1088/1742-6596/1159/1/012017 (2019).

[15] J. A. Stratton, *Electromagnetic Theory* (McGraw-Hill, 1941).